2017

Asteroseismic analysis of the pulsating subdwarf B star KIC 11558725: an sdB+WD system with divergent frequency multiplets and mode trapping observed by Kepler

J W. Kern
MSU Graduate Student

Michael D. Reed
Missouri State University

A S. Baran
Missouri State University

J. H. Telting

R H. Østensen
Missouri State University

Recommended Citation

Kern, J. W., M. D. Reed, A. S. Baran, J. H. Telting, and R. H. Østensen. "Asteroseismic analysis of the pulsating subdwarf B star KIC 11558725: an sdB+ WD system with divergent frequency multiplets and mode trapping observed by Kepler." Monthly Notices of the Royal Astronomical Society 474, no. 4 (2018): 4709-4716.

Monthly Notices
of the
ROYAL ASTRONOMICAL SOCIETY

MNRAS **474,** 4709–4716 (2018)
Advance Access publication 2017 November 10

doi:10.1093/mnras/stx2893

Asteroseismic analysis of the pulsating subdwarf B star KIC 11558725: an sdB+WD system with divergent frequency multiplets and mode trapping observed by *Kepler*

J. W. Kern,[1★] M. D. Reed,[1★] A. S. Baran,[1,2] J. H. Telting[3] and R. H. Østensen[1]

[1]*Department of Physics, Astronomy and Materials Science, Missouri State University, 901 S. National, Springfield, MO 65897, USA*
[2]*Suhora Observatory and Krakow Pedagogical University, ul. ży ch 2,PL-30-084 Kraków, Poland*
[3]*Nordic Optical Telescope, Rambla José Ana Ferréndez Pérez 7, E-38711 Breña Baja, Spain*

Accepted 2017 November 6. Received 2017 November 3; in original form 2017 August 24

ABSTRACT

We analyse the full *Kepler* short cadence data set of the pulsating subdwarf B star KIC 11558725. KIC 11558725 is in an sdB+WD binary system with a period of 10.05 d and is known to be subsynchronously rotating. From the full data set, we detected 245 pulsation frequencies, mostly in the gravity (g-) mode region, but some in the pressure (p-) mode region as well. We are able to identify 142 of these pulsations as $\ell \leq 2$ modes and 27 as $\ell = 6$ modes. Frequency splittings in the g- and p-mode regions indicate that KIC 11558725 is a solid-body rotator with a rotation period of ∼44 d. The $\ell = 6$ multiplets do not show a constant splitting, with the splitting increasing over the course of the observations. Multiplet structure constrains the inclination of the pulsation axis to be greater than ∼80°. KIC 11558725 also displays mode trapping in two regions of its asymptotic sequence.

Key words: stars: oscillations – subdwarfs.

1 INTRODUCTION

Subdwarf B (sdB) stars are extreme-horizontal-branch stars of $\sim 0.5\,M_{\odot}$, $20\,000 \lesssim T_{\rm eff} \lesssim 40\,000$ K and $5.0 \lesssim \log g \lesssim 6.0$. Pulsators (sdBV stars) have been discovered with short (periods of a few minutes) and long (periods of an hour or two) periods associated with pressure and gravity modes, respectively (Kilkenny et al. 1997; Green et al. 2003). Gravity (g-) mode pulsations are deep interior modes, which exhibit asymptotic period spacings for radial nodes with $\ell \ll n$ (Reed et al. 2011), whereas pressure (p-) modes mostly sample the envelope (Charpinet et al. 2000). For a comprehensive review of sdB stars, see Heber (2016).

Thanks to the continuous, long-duration nature of *Kepler* data, observational constraints on sdBV stars, mostly pertaining to the identifications of non-radial pulsation modes, have been obtained. Non-radial pulsations can be characterized by three quantum integers: n (radial order), ℓ (spherical degree) and m (azimuthal degree). The two most prominent identification methods rely on asymptotic g-mode period spacings (Reed et al. 2011) and rotationally induced frequency multiplets (Baran et al. 2012). Observed smooth asymptotic period sequences indicate a homogeneous pulsation cavity, whereas traditional structural models indicate sharp boundaries at the C–O/He and He/H transition regions. The solution may be increased diffusion (Hu et al. 2008; Constantino et al. 2015; Ghasemi et al. 2017), which smooths the He/H transition. In some stars, the asymptotic g-mode sequences are interrupted by trapped modes (Østensen et al. 2014; Foster et al. 2015; Kern et al. 2017). These trapped modes may be a result of convective overshoot in the C–O/He transition layer, as shown by Constantino et al. (2015) and Ghasemi et al. (2017).

Frequency multiplets allow mode identifications as each degree will produce $2\ell + 1$ azimuthal m modes, so $\ell = 1$ modes produce triplets, $\ell = 2$ modes produce quintuplets, and so on. In addition, the frequency separations are related to the star's rotation $\Delta\nu = \Delta m \Omega (1 - C_{n,\ell})$ where Ω is the rotational frequency and $C_{n,\ell}$ is the Ledoux constant (Ledoux 1951), which is $C_{n,\ell} \approx \frac{1}{\ell(\ell+1)}$ for g modes and very small for p modes. Rotation periods have generally been found to be 10 to 100 d (Reed et al. 2014), even when in binaries with periods down to half a day (Pablo, Kawaler & Green 2011; Baran & Winans 2012). In the fortunate case of a hybrid pulsator with frequency splittings in both g and p modes, they allow an independent determination of core and envelope rotation. To date, two sdB stars have been shown to be solid-body rotators (Baran et al. 2012; Kern et al. 2017) and two others to be radially differential rotators (Foster et al. 2015; Baran et al. 2017).

The determination of rotation periods from multiplet frequency splittings is grounded in the assumption that frequency multiplets are driven by rotation. However, changing frequency splittings found in two sdBV stars, Balloon 090100001 (Baran et al. 2009) and KIC 2697388 (Kern et al. 2017), challenge the idea that rotation

★ E-mail: Kern28@live.missouristate.edu (JWK); mikereed@missouristate.edu (MDR)

is solely responsible for the splittings. Two proposed mechanisms for modifying rotational splittings are angular momentum exchange between rotation and pulsations (Pérez, Oreiro & Hu 2011) and, a purely pulsational effect, resonant mode coupling (Zong, Charpinet & Vauclair 2016). Considering the frequency splittings should go to zero within a decade, neither mechanism provided a reasonable solution (Kern et al. 2017). Even the possibility of external torques from a binary partner is unlikely with a radial velocity signal less than 9 $km{\cdot}s^{-1}$ (Kern et al. 2017).

Following the successes of previous seismic analyses of Kepler data of sdBV stars, this paper examines data for KIC 11558725. Previous analyses of KIC 11558725 include the discovery of asymptotic g-mode sequences with period spacings of 247 and 143 s for $\ell = 1$ and 2 modes, respectively (Reed et al. 2011), and an analysis by Telting et al. (2012) of 15 months (Q6–Q10) of Kepler data. Telting et al. (2012) detected 168 frequencies, confirmed the asymptotic sequences, and, in combination with spectroscopic observations, used three different methods (Doppler-beaming, radial-velocities and pulsation timing) to determine a binary period of 10.05 d. Mode identifications were assigned to 98 frequencies, mostly of low-degree (ie: $\ell = 1$ or 2). Telting et al. (2012) also used the rotationally induced frequency splittings in the g-mode region to determine a rotation period of roughly 45 d; indicating it to have subsynchronous rotation compared to the binary period.

In this paper, we present our analyses of the entire 35 month *Kepler* data set of KIC 11558725.

2 DATA PROCESSING AND ANALYSIS

We used the standard data processing techniques described in many of the previous analysis of *Kepler* sdBV stars (e.g. Reed et al. 2014; Foster et al. 2015; Kern et al. 2017). Briefly, we downloaded the *Kepler* short cadence data from the Mikulski Archive for Space Telescopes (MAST). We obtained data from quarters 6 (Q6) through Q17. In total, we accrued ∼1.4 million observations spanning a total time of ∼1051.5 d with a duty cycle of 91 per cent. We removed long-term trends, used the mean brightness to normalize the data and sigma-clipped the data at 5σ. We converted the luminosity intensities into parts-per-thousand (ppt) and combined into one resultant light curve spanning ∼3 yr. Finally, we used the orbital parameters from Telting et al. (2012) to correct for the Rømer delay.

In order to determine pulsation frequencies, we exploit the nearly evenly spaced *Kepler* data by taking a Fourier transform (FT) of the light curve. The $1.5/T$ temporal resolution (Loumos & Deeming 1978) was determined to be 0.018 μHz. In order to ensure that a pulsation is intrinsic to the star and not noise, this temporal resolution requires a detection threshold of 4.8σ (Bevington & Robinson 2003), which we calculate to be 0.0196 ppt. Fig. 1 shows the final FT of the full data set.

To evaluate the temporal evolution of pulsations, we created subsets of data of two types. The first subsets spanned nine months stepped by three months and were inspected individually. The second are sliding FTs (sFTs) using data spanning 200 d stepped by 5 d. The $1.5/T$ temporal resolution of these data sets are 0.0868 and 0.0634 μHz, respectively, small enough to resolve rotation multiplets.

We searched the full data set, the nine month subsets and the sFTs for significant pulsation frequencies. A total of 25 pulsations that were mostly constant in frequency and amplitude were pre-whitened from the light curve. The remaining peaks varied in frequency and/or amplitude over the course of observations and were fitted with Lorentzian profiles using the Lorentzian widths as frequency

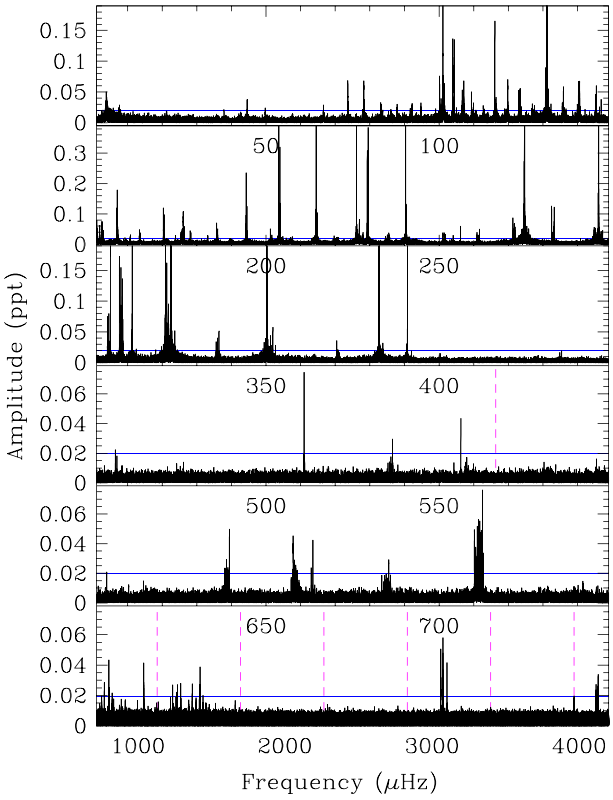

Figure 1. FTof the entire data set. The blue horizontal line is the detection limit and vertical (magenta) dashed lines indicate known spacecraft artefacts. In order to more clearly show the pulsations, some amplitudes are truncated. The top three panels have different amplitude scales and the bottom panel has a different frequency scale.

errors. In an effort to measure accurate frequency splittings, multiplets are extracted when all of the peaks are excited simultaneously. However, this does not necessarily correlate to when the pulsations are at their highest amplitudes, so some of the pulsations in our final list have signal-to-noise ratios (S/N) lower than our detection threshold. Any other pulsations with amplitudes lower than 4.8σ are supported by either frequency splittings or period sequences. In total, 245 pulsation frequencies were fitted: 166 gravity modes (30–400 μHz), 66 intermediate modes (400–1500 μHz) and 13 pressure modes (1500 to ∼8000 μHz). A small excerpt of our frequency list is given in Table 1 with the full list available online.

3 RESULTS

We use the entire *Kepler* data set of KIC 11558725 to investigate mode identifications and the temporal evolution of its pulsations, and detect 78 more frequencies than Telting et al. (2012).

3.1 Rotationally induced frequency multiplets

Telting et al. (2012) detected $\ell = 1$ multiplets with splittings near 0.13 μHz. We began our multiplet analysis in the g-mode region by finding frequencies separated by ∼0.13 μHz and twice that, as Telting et al. (2012) also found many $\Delta m = 2$ multiplets. Most of the highest amplitude frequencies show these splittings, as expected, since $\ell = 1$ modes have the lowest geometric cancellation (Pesnell 1985). Since we know there are lots of $|m| = 1$ doublets, for doublets with $\Delta m = 1$ splittings ($\ell, m = 1, 0$ and $1, |1|$), we arbitrarily assign the lowest amplitude as the $m = 0$ component. In total, we found

Table 1. Excerpt of the full list of KIC 11558725's periodicities. (Complete table is available online as Supporting Information.) Errors are given in parentheses. Asterisks on frequency IDs indicate the pulsation was pre-whitened from the light curve. Column 4 refers to the data set in which the pulsation was fit. Data sets starting with Q span three months, whereas All represents the entire data set. Column 6 refers to the mode identifications from this work. Asterisks on mode identifications indicate trapped modes. Column 7 provides the mode identifications from Telting et al. (2012). Column 8 provides the deviations from asymptotic period spacings, and column 9 lists the $\Delta m = 1$ frequency splittings.

ID	Frequency (μHz)	Period (s)	Set	S/N	Mode (this work) ℓ, m, n	Mode (Telting) ℓ, n	$\frac{\Delta P}{\Delta \Pi}$ (per cent)	$\Delta\nu$ (μHz)
f105*	305.029 64 (0.00007)	3278.3699 (0.0008)	All	55.28	2, 2, 17*			
f106	304.610 (0.019)	3282.89 (0.205)	Q7	12.19	2, 0, 17*			0.210
f107	304.195 (0.022)	3287.37 (0.238)	Q7	9.41	2, −2, 17			0.208
f108*	296.106 36 (0.00001)	3377.1648 (0.0002)	All	213.21	1, –, 8	1, 8/2, 18	10.3	
f109	283.257 (0.024)	3530.36 (0.299)	Q12	12.62	2, 2, 19	2, 19	7.4	
f110	282.905 (0.033)	3534.76 (0.412)	Q12	10.33	2, 0, 19	2, 19	4.2	
f111	282.528 (0.023)	3539.47 (0.288)	Q12	20.35	2, −2, 19	2, 19	0.9	
f112*	274.752 87 (0.00002)	3639.6344 (0.0003)	All	172.29	1, 0, 9	1, 9	4.5	
f113*	274.641 87 (0.00002)	3641.1054 (0.0002)	All	233.00	1, −1, 9	1, 9	3.9	0.111
f114	272.019 (0.021)	3676.21 (0.284)	Q14	8.78	2, 2, 20	2, 20	5.5	
f115	271.671 (0.046)	3680.92 (0.623)	Q14	7.57	2, 0, 20	2, 20	2.2	
f116	271.321 (0.024)	3685.67 (0.326)	Q14	9.16	2, −2, 20	2, 20	1.2	
f117	261.656 (0.021)	3821.81 (0.307)	Q14	12.50	2, 2, 21		3.9	
f118	261.276 (0.016)	3827.37 (0.234)	Q14	4.93	2, 0, 21		0.1	0.190
f119	260.928 (0.020)	3832.47 (0.294)	Q14	6.04	2, −2, 21		3.7	

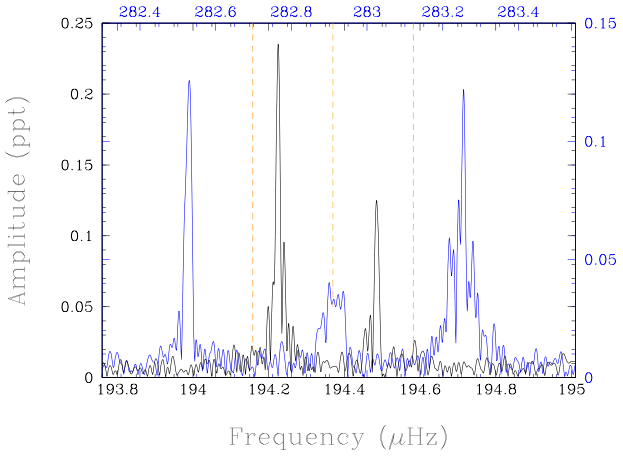

Figure 2. An $\ell = 1$ doublet at ∼194 μHz (black), and an $\ell = 2$ triplet at ∼283 μHz (blue). The three dashed lines indicate the $m = -1$, 0 and 1 components for $\ell = 2$. Both multiplets are centred about $m = 0$.

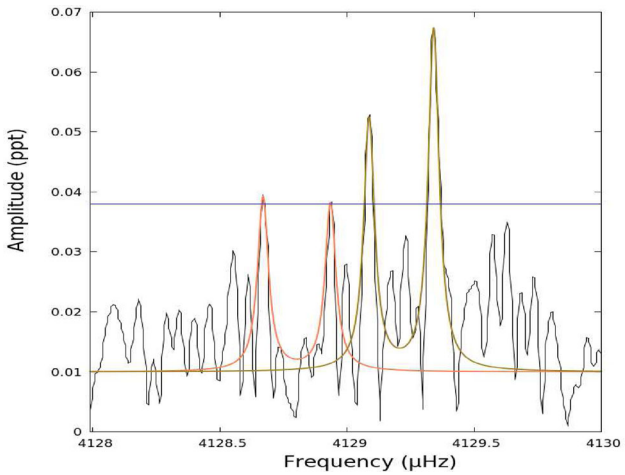

Figure 3. Two *p*-mode doublets near 4129 μHz in Q12–Q14. Each doublet is shown with its Lorentzian profile where the horizontal line is the detection threshold.

27 $\ell = 1$ splittings with an average of 0.131 ± 0.023 μHz. We also discovered a set of high-amplitude triplets with splittings near 0.404 μHz. With $\ell = 1$ splittings of 0.131 μHz, the corresponding $\ell = 2$ splitting is 0.218 μHz. Thus, we interpret the triplet structures as the $m = 0$ and $|m| = 2$ components of $\ell = 2$ quintuplets. We find a total of 26 $\ell = 2$ splittings with an average $\Delta m = 1$ value of 0.210 ± 0.021 μHz. The observed $\ell = 1$ to 2 ratio of the frequency splittings is 0.624, which is within 2.5 per cent of the theoretical value (Ledoux 1951). An example of the multiplet structure for $\ell = 1$ and 2 is shown in Fig. 2.

We also inspected the p-mode region and extracted 13 significant frequencies, twice as many as the previous result. Multiplet structure is seen in 54 per cent of these pulsations, an example of which is shown in Fig. 3. Frequency splittings were extracted from multiplets centred at roughly 4126, 4128.8 and 4129.2 μHz, in which a common splitting of 0.288 ± 0.022 μHz was discovered. The frequency splittings in the p- and g-mode regions agree with Ledoux theory to within ∼10 per cent assuming $C_{n,\ell} \sim 0$ for p modes.

The remaining 27 per cent of pulsations lie between the p- and g-mode regions from 400 to 1500 μHz. The highest amplitude pulsations in this region are located at roughly 658 and 711 μHz and show clear higher order multiplet structure with as many as seven identifiable peaks. An example is shown in Fig. 4. The frequency splittings from these mulitplets in Q6–Q8 are approximately 0.394 μHz, too large for $\Delta m = 1$ regardless of their degree, ℓ. In total, we found 27 frequencies in this region with splittings that average to 0.222 ± 0.044 μHz for $\Delta m = 1$. This is just slightly larger than the $\ell = 2$ g-mode splittings. Since we interpret the observed splittings as $\Delta m = 2$, the full multiplet at 711 μHz would have a total of 13 peaks and a mode identification of $\ell = 6$. Like $\ell = 6$ modes, their radial indices (see Section 3.3) match those of low-degree g-modes.

3.2 Frequency and temporal dependence of multiplets

Intriguingly, the g-mode $\ell = 1$ multiplet structure shows a transition from $\Delta m = 1$ to 2 from high to low frequencies. Between 400 and

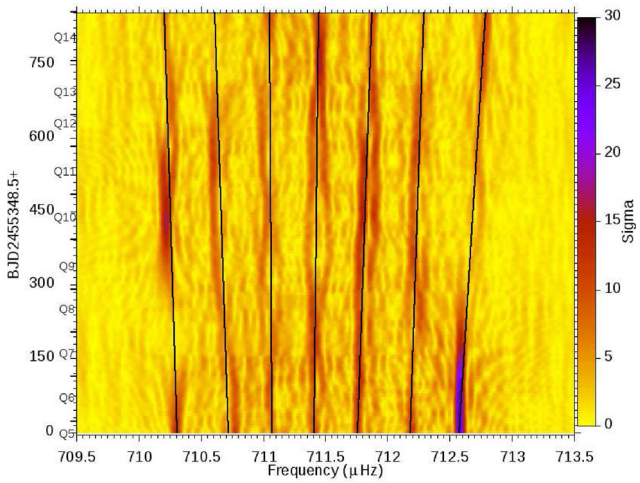

Figure 4. s FTshowing the time evolution of an ℓ, $n=6$, 14 multiplet. At ∼711 μHz, the frequency splittings are diverging at a rate of 0.016 ± 0.002 μHz yr^{-1}.

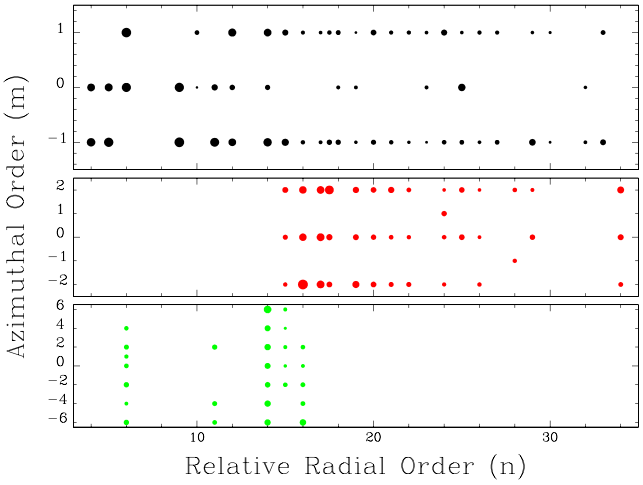

Figure 5. Radial order plotted against azimuthal order showing the radial (frequency) dependence of the $\ell = 1$ (black) multiplets compared to the $\ell = 2$ (red) and $\ell = 6$ (green) multiplets. The size of each point represents its amplitude.

240 μHz, there are six doublets that have splittings of $\Delta m = 1$. This transitions with two triplets near 229 and 204 μHz, which have strong $|m| = 1$ components and comparatively weak central $m = 0$ components. Below 200 μHz, doublet structures of $\Delta m = 2$ dominate. Fig. 5 shows a plot of m-components plotted against relative radial order, n (described in Section 3.3), for all pulsation modes. With only two exceptions, the $\ell = 2$ multiplets only show $\Delta m = 2$ splittings. Similarly, the $\ell = 6$ multiplets only have $\Delta m = 2$ splittings excepting a single ℓ, $m = 6$, 1 at $n = 6$.

Interestingly, the $\ell = 6$ multiplets exhibit an increase in their frequency splittings over the duration of *Kepler* observations; this divergence is shown in Fig. 4. This is the first instance of diverging frequency splittings found in any *Kepler* sdB pulsator. Changing frequency splittings, both divergent and convergent have been observed in two other sdB pulsators (Baran et al. 2008 and Kern et al. 2017, respectively). In a manner similar to Kern et al. (2017), we fitted the frequencies during early observations (Q6–Q9) and late observations (Q13–Q17), calculated the rate of change and

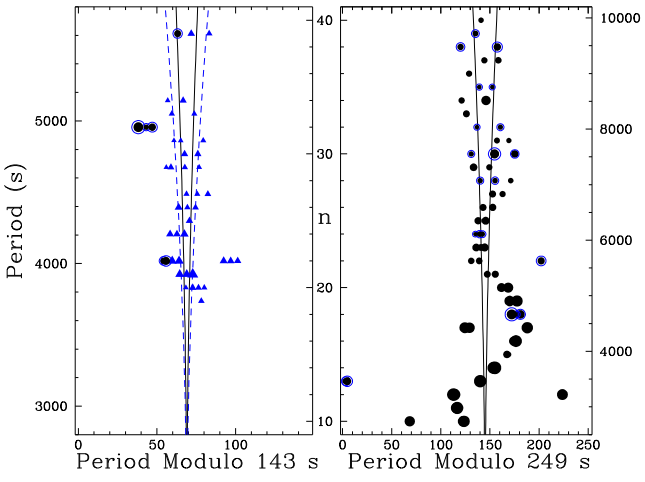

Figure 6. Echelle diagram containing only the g-mode pulsations from $n = 9$ to 41. The period modulo for $\ell = 1$ is plotted on the right-hand side and $\ell = 2$ is on the left-hand side. Black dots are $\ell = 1$, blue triangles are $\ell = 2$ and black dots with blue circles have characteristics of both $\ell = 1$ and 2. The amplitude of each peak is given by the size of the data point.

provide the results in Table 2. We also provide values for $\ell = 1$ and 2 multiplets, which are consistent with no change.

Unlike for KIC 2697388 (Kern et al. 2017), the rate is not the same between the multiplets. The divergence rates of $\ell = 6$ multiplets with $n = 16$, 15 and 14 are roughly 0.015 μHzyr^{-1} for $\Delta m = 1$, and all agree within their errors. However, this divergence rate slows to 0.009 μHz yr^{-1} for $n = 11$, and 0.007 μHz yr^{-1} for $n = 6$.

3.3 Asymptotic period spacing and mode trapping

Observed asymptotic period spacings provide a well-established tool for mode identification in pulsating sdB stars with which Reed et al. (2011) and Telting et al. (2012) found $\ell = 1$ and 2 spacings of 248.7 and 143.4 s, respectively. We independently determined period spacing sequences. Using our mode identifications from frequency splittings, we looked at period differences between the $m = 0$ components of the multiplets to determine period sequences. We assigned relative radial overtones, n, which have an arbitrary offset and then iteratively added periods which fit our $\ell = 1$ and 2 sequences. We were able to identify two, well-defined period spacing sequences for $\ell = 1$ and 2 of 244.45 ± 0.32 and 144.04 ± 0.46 s, respectively. These are in agreement with previous values (Reed et al. 2011; Telting et al. 2012). The ratio of these two spacings is 1.697, which also agrees with Ledoux theory within 1 per cent (Ledoux 1951). These asymptotic period spacings identified 60 $\ell = 1$ and 67 $\ell = 2$ pulsations as well as their relative radial indices.

We then used amplitude-weighted echelle diagrams to visually inspect the period sequences for mode trapping or holistic trends. Echelle diagrams plot the period modulo against period. Pulsations driven on a sequence have nearly equal period spacings and are vertically aligned in the plot. The most notable feature in the echelle diagram for the $\ell = 1$ sequence is the large 'hook' feature between 3000 and 6000 s, which can be seen in the right-hand plot in Fig. 6.

It is in the region from $n = 8$ to 35 that we see a nearly complete sequence of consecutive radial nodes with only one missing node at $n = 12$. However, we also see the trapping of two high amplitude modes at ∼4360 s in between $n = 11$ and 12. The high amplitude nature of these peaks and their multiplet structure allow us to identify these as $\ell = 1$ pulsations. In the $\ell = 2$ sequence, from

Table 2. Divergence rates of all $\ell = 6$ multiplets and selected $\ell = 1$ and 2 multiplets. The low-degree modes were chosen to be in a similar range of radial orders as that of the high-degree modes. Column 4 shows the $\Delta m = 1$ frequency splittings.

ℓ, n	Frequency splittings Q6–Q9 (μHz)	Frequency splittings Q13–Q17 (μHz)	$\Delta\nu$ / Δt (μHz yr^{-1})
1, 14	0.161 (0.036)	0.157 (0.034)	−0.002 (0.050)
1, 15	0.124 (0.035)	0.127 (0.038)	0.002 (0.052)
1, 16	0.141 (0.029)	0.133 (0.030)	−0.004 (0.042)
1, 17	0.145 (0.033)	0.133 (0.034)	−0.006 (0.047)
1, 18	0.128 (0.038)	0.129 (0.035)	0.001 (0.052)
Total rate of $\ell = 1$			−0.002 (0.022)
2, 15	0.197 (0.020)	0.210 (0.016)	0.007 (0.026)
2, 16	0.208 (0.015)	0.224 (0.016)	0.008 (0.022)
2, 17	0.198 (0.018)	0.207 (0.019)	0.005 (0.026)
2, 19	0.173 (0.019)	0.179 (0.019)	0.003 (0.027)
2, 20	0.164 (0.020)	0.172 (0.015)	0.004 (0.025)
Total rate of $\ell = 2$			0.005 (0.011)
6, 6	0.264 (0.006)	0.279 (0.010)	0.007 (0.011)
6, 11	0.153 (0.010)	0.168 (0.008)	0.009 (0.009)
6, 14	0.184 (0.003)	0.211 (0.003)	0.016 (0.002)
6, 15	0.189 (0.003)	0.216 (0.005)	0.016 (0.003)
6, 16	0.198 (0.004)	0.232 (0.005)	0.015 (0.003)
Total rate of $\ell = 6$			0.015 (0.001)

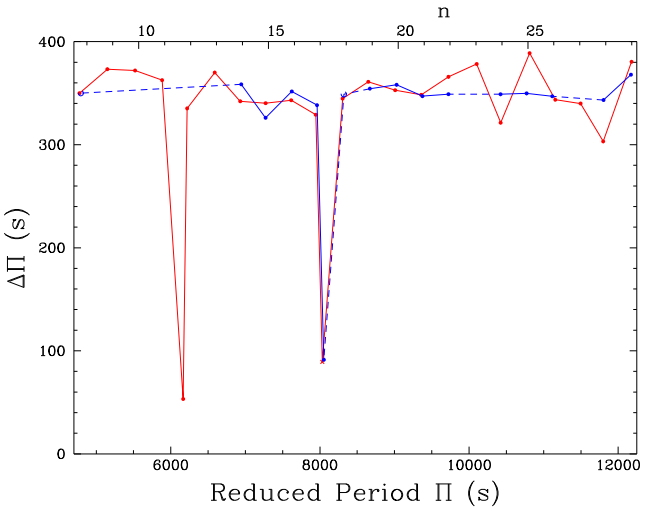

Figure 7. Reduced-period plot indicating mode trapping in both the $\ell = 1$ (red) and $\ell = 2$ (blue) sequences. Solid lines connect consecutive overtones, whereas dashed lines indicate missing members in the sequence.

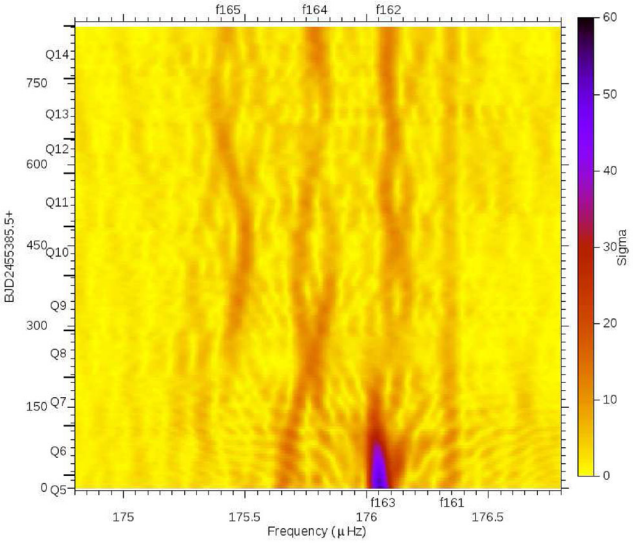

Figure 8. sFTof the trapped n, $\ell = 17$, 1 doublet (f161 and f163) overlaying an asymptotic n, $\ell = 34$, 2 triplet (f162, f164 and f165).

$n = 14$ to 29, we see the most consecutive radials nodes with only two missing at $n = 18$ and 23. Similar to the $\ell = 1$ sequence, mode trapping is also seen at ∼3280 s in between $n = 17$ and 18. These trapped modes are shown in the left-hand plot of Fig. 6. No trapped mode was found to correspond to the missing $n = 23$.

Mode trapping affects all pulsations at the same radial nodes regardless of their degree. Therefore, we searched for the $\ell = 2$ and 1 counterparts to our independently identified trapped $\ell = 1$ and 2 pulsations. As an aide for our search, we calculated reduced periods. The periods contained in any g-mode period sequence are dependent on ℓ, but can become ℓ-independent by multiplying each period by $\sqrt{\ell(\ell+1)}$. This aligns the radial nodes of each sequence, making them degenerate. Consequently, when reduced period is plotted (shown in Fig. 7) against the reduced period spacings, trapped modes appear as very large deviations from the average spacing near ∼350 s.

The trapped $\ell = 2$ pulsation (seen in the left-hand plot of Fig. 6 at ∼3280 s) is seen as the large, blue trough at the reduced period of ∼8050 s in Fig. 7. Determining its potential $\ell = 1$ counterpart should be driven with a period of ∼5690 s, we searched and found a group of frequencies with $\ell = 1$ and 2 properties (shown in Fig. 8) at ∼5680 s or ∼176 μHz.

This group has five frequencies, labelled f165–f161, in which f165, f164 and f162 show similar frequency variations, whereas f161 stays constant. At 176.05 μHz, there is a very large amplitude near time zero, labelled f163, which fades out quickly and is just shortwards (left-hand side) of f162. The splitting between f161 and f163 is 0.282 μHz, which fits an $\ell, m = 1, |1|$ doublet with $\Delta m = 2$,

in agreement with most of our observed $\ell = 1$ multiplets. Thus, it is our interpretation that f161 and f163 are the trapped $\ell = 1$ pulsation corresponding to the trapped $\ell = 2$ pulsation at ∼3280 s. No corresponding trapped $\ell = 2$ was found for the trapped $\ell = 1$ pulsation at ∼4360 s.

4 SUMMARY AND DISCUSSION

We discovered five things from our analyses of the complete *Kepler* short cadence data set (Q6–Q17), mode trapping, a transition from $\Delta m = 1$ to 2 for low radial order $\ell = 1$ pulsations, constraints on the inclination axis, solid-body rotation and diverging frequency splittings for $\ell = 6$ multiplets, whereas $\ell = 1$ and 2 multiplet frequencies remain constant. We detected 245 pulsation frequencies: 166 in the heart of the g-mode region between 30 and 400 μHz, 66 between 400 and 1500 μHz, including some high-degree g-modes, and 13 p-modes between 1500 μHz and the Nyquist frequency. We recovered 96 per cent of those found by Telting et al. (2012), including 25 out of the 32 possible combination frequencies. The remaining 4 per cent were above the 4σ detection threshold stated in Telting et al. (2012) during Q6–Q10; however, they were below our 4.8σ detection threshold and were undetected in Q11–Q17; therefore, we excluded these from our final list. Using asymptotic period spacing and frequency multiplets, we were able to identify 168 pulsations with mode identifications: 60 $\ell = 1$, 57 $\ell = 2$, 24 $\ell = 1$ or 2, and 27 $\ell = 6$. A comprehensive list of the pulsation frequencies and our final mode identifications are given in the online material.

Telting et al. (2012) listed 12 combinations of frequencies for which F3–F2–F1 = 0, and suggested that these combinations may be due to modal interaction intrinsic to the star. A requirement for such interaction is that the frequency combinations still hold in the corotating frame of the star, implying that the azimuthal modes of a given combination must be degenerate. Inspecting our mode identifications, we find four combinations have sufficient mode identifications to test for possible modal interactions, and in no case were the azimuthal modes degenerate. This means that the frequencies do not combine in the corotating frame of the star hence two explanations remain for the observed combinations; they are either by chance or they are an observational effect due to the non-linear addition of the observed quantities. Telting et al. (2012) tested the former possibility using simple Monte Carlo statistical modelling and found that only 4 out of 12 such combinations are expected by chance. Thus, we find no evidence that the frequency combinations are due to intrinsic modal interactions.

Our analyses confirmed the asymptotic period spacings in the g-mode region found by Telting et al. (2012) ($\ell = 1$ and 2 of 244.45±0.32 and 144.04±0.46 s, respectively); however, previously unidentified mode trapping was discovered at two relative radial nodes, $n = 12$ and 17. Trapped modes have previously been found in four other *Kepler* sdBV stars (Østensen et al. 2014; Foster et al. 2015; Kern et al. 2017, Baran et al. 2017) and likely are sensitive to core conditions. Recent work using MESA evolutionary models (Paxton et al. 2011) indicates that convective overshoot or semiconvection can produce the observed trapping structures at the C–O/He boundary. (Constantino et al. 2015; Ghasemi et al. 2017). Indeed, Ghasemi et al. (2017) were able to exactly match the asymptotic period sequence and trapped modes in KIC 10553698A using diffusion at the He/H boundary and modest convective overshooting at the C–O/He boundary.

We confirm the multiplet frequency splittings of Telting et al. (2012) but uncover new features. An interesting feature in the $\ell = 1$ frequency splittings is the radial dependence of the azimuthal components. For KIC 11558725, 56 per cent of its pulsations lie between 100 and 400 μHz, in which half are identified as $\ell = 1$ pulsations. The $\ell = 1$ azimuthal components transition from $\Delta m = 1$ to 2 in the range of relative radials nodes from $n = 5$ to 33. The inclination of the pulsation axis affects the observed amplitude ratios of frequencies in a multiplet (Pesnell 1985), and multiple pulsation axes have been discovered in cases of strong tidal forces (Reed et al. 2011) or strong magnetic fields (Kurtz et al. 2011). However, the $\ell \geq 2$ modes do not show the same trend, tidal forces for KIC 11558725 are much weaker and sdB stars have been found to have weak magnetic fields (O'Toole et al. 2005). Thus, this phenomenon is more likely some selection effect of the driving mechanism, though detailed modelling would be required to determine if this is so.

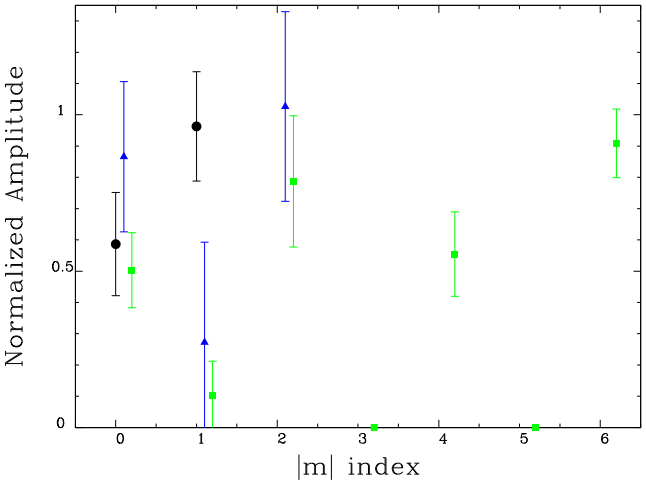

Figure 9. Plot showing the normalized amplitude of the azimuthal components of all ℓ-degrees. The $\ell = 1$ components are the black circles, $\ell = 2$ components are blue triangles and $\ell = 6$ components are green squares.

In general, the odd m-components of the $\ell = 2$ and 6 multiplets are not observed, whereas the $\ell = 1$ multiplets have predominantly small $m = 0$ peaks, shown in Fig. 9. The amplitudes were normalized to the strongest pulsation in a given multiplet. Since the $\ell = 1$ multiplet structure changes with radial order, the pulsation axis is only constrained to $i \gtrsim 37^\circ$. However, the $\ell = 2$ and 6 multiplet structures constrain the pulsation axis to be $i \gtrsim 72^\circ$ and 80° , respectively, as shown in Fig. 10. Telting et al. (2012) determined that eclipses would occur for $i > 88^\circ$ and so we can constrain the pulsation axis as $80^\circ \lesssim i < 88^\circ$.

We assume the high-degree multiplets to be $\ell = 6$, since $\ell < 6$ would not have sufficient multiplet members and we presume symmetry about the $m = 0$ component. $\ell = 7$ is also possible if only odd components are observed and one of the $|m| = 7$ peaks is missing. Both fit the inclination constraints that are seen in the bottom panels of Fig. 10.

Our analysis also uncovered new information about the bulk rotation of the star. The g-mode frequency splittings for $\ell = 1$ and 2 multiplets correspond to a core rotation period of 45.1 ± 7.8, which is consistent with the p-mode-determined envelope rotation period of 40.2 ± 3.3 d. As such, we interpret KIC 11558725 to be a solid-body rotator with a rotation period of ∼44 d. We did not use the $\ell = 6$ multiplets for this calculation since they diverge over the course of observations.

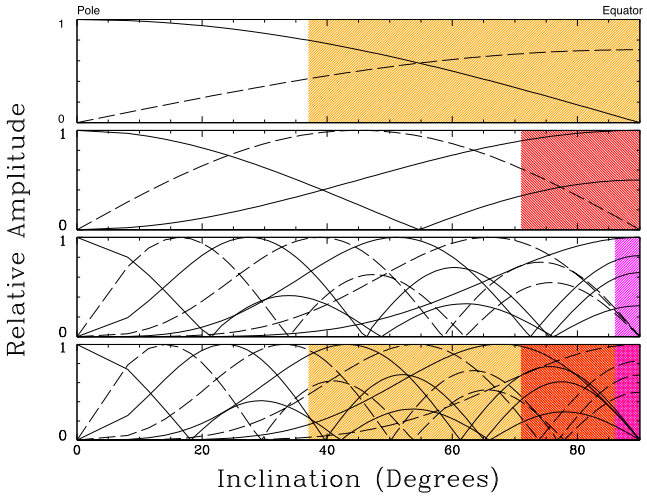

Figure 10. The Legendre polynomials depicting the normalized amplitudes of each peak in a multiplet of a given ℓ-degree, $\ell = 1$ are given in the top panel, $\ell = 2$ in the second panel, $\ell = 6$ in the third panel and $\ell = 7$ in the bottom panel. The solid lines represent even components, whereas the dashed lines represent odd components. The orange, red and magenta shaded areas are the constrained inclinations given by the amplitudes of peaks within the observed $\ell = 1$, 2 and 6 multiplets, respectively. The constraints are plotted on the Legendre polynomials for $\ell = 7$ for reference.

The divergence of the frequency splittings for the $\ell = 6$ multiplets is a very interesting result. The only other *Kepler* sdBV (KIC 2697388) known to have changing frequency splittings was discovered last year by our collaboration (Kern et al. 2017). In that case, the $\ell = 2$ and 4 multiplets were converging, whereas the $\ell = 1$ multiplets appeared constant. In this study, we find the $\ell = 6$ multiplets to be *diverging*, whereas the $\ell = 1$ and 2 multiplets are constant. Additionally, the convergence rate for KIC 2697388 was constant across multiplets, whereas KIC 11558725's divergence rate slows down with increasing frequency (Table 2). We note that the rates are similar between the two stars with KIC 2697388's converging frequencies reaching zero separation within a decade, whreas KIC 11558725's largest diverging frequencies would have had zero separation about 16 yr ago, assuming constant rates for both stars. We interpret this similarity of time-scale to indicate a common cause. We also notice that the $\ell = 8$ multiplet of KIC 7668647 shown in fig. 9 of Telting et al. (2014) may be converging.

Mechanisms for modifying multiplet splittings include angular momentum exchanges between rotation and pulsations (Pérez et al. 2011), resonant mode coupling (Zong et al. 2016), strong magnetic fields (e.g. Kurtz et al. 2011) and rotation. Rotation can be ruled out since KIC 11558725's $\ell = 1$ and 2 multiplets are constant. As previously mentioned, sdB stars seem to have weak magnetic fields (O'Toole et al. 2005), making that an unlikely cause. Kern et al. (2017) discussed why the remaining two mechanisms were unlikely for KIC 2697388, and we find the same results for KIC 11558725.

The exchange of angular momentum between rotation and pulsation should drive differential rotation between the g and p modes, basically the g-mode angular momentum goes into the envelope that changes the rotation there in a periodic way, modifying p-mode multiplets. The exchange of energy also produces a change in the g-mode pulsation amplitudes, depending on the direction the energy is going (Pérez, private communication). However, we are observing g-mode frequency modifications rather than p-mode ones, so this does not appear to be the mechanism. Resonant mode coupling establishes changes in frequency over a period of modulation (Zong et al. 2016). Based on our measured frequency splittings and their rates of change, the period of modulation for KIC 11558725 would be roughly 373 d, an order of magnitude larger than we observe. In a similar manner to KIC 2697388, the four mechanisms fail to accurately explain the observed change in frequency splittings making for another fascinating and enigmatic result.

ACKNOWLEDGEMENTS

Funding for this research was provided by the National Science Foundation grant#1312869. Any opinions, findings, and conclusions or recommendations expressed in this material are those of the author(s) and do not necessarily reflect the views of the National Science Foundation. ASB gratefully acknowledges a financial support from the Polish National Science Center under project No. UMO-2011/03/D/ST9/01914. This paper includes data collected by the *Kepler* mission. Funding for the *Kepler* mission is provided by the NASA Science Mission directorate. Data presented in this paper were obtained from the Mikulski Archive for Space Telescopes (MAST). STScI is operated by the Association of Universities for Research in Astronomy, Inc., under NASA contract NAS5-26555. Support for MAST for non-*HST* data is provided by the NASA Office of Space Science via grant NNX13AC07G and by other grants and contracts.

REFERENCES

Baran A. S., Winans A., 2012, Acta Astron., 62, 343
Baran A., Pigulski A., O'Toole S. J., 2008, MNRAS, 385, 255
Baran A. et al., 2009, MNRAS, 392, 1092
Baran A. S. et al., 2012, MNRAS, 424, 2686
Baran A. S., Reed M. D., Østensen R. H., Telting J. H., Jeffery C. S., 2017, A&A, 597, A95
Bevington P. R., Robinson D. K., 2003, Data Reduction and Error Analysis for the Physical Sciences. McGraw-Hill, Boston, MA
Charpinet S., Fontaine G., Brassard P., Dorman B., 2000, ApJS, 131, 223
Constantino T., Campbell S., Christensen-Dalsgaard J., Lattanzio J., Stello D., 2015, MNRAS, 452, 123
Foster H. M., Reed M. D., Telting J. H., Østensen R. H., Baran A. S., 2015, ApJ, 805, 94
Ghasemi H., Moravveji E., Aerts C., Safari H., Vuckovic M., 2017, MNRAS, 465, 1518
Green E. M. et al., 2003, ApJ, 583, L31
Heber U., 2016, PASP, 128, 082001
Hu H., Dupret M., Aerts C., Nelemans G., Kawaler S. D., Miglio A., Montalban J., Scuflaire R., 2008, A&A, 490, 243
Kern J. W., Reed M. D., Baran A. S., Østensen R. H., Telting J. H., 2017, MNRAS, 465, 1057
Kilkenny D., Koen C., O'Donoghue D., Stobie R. S., 1997, MNRAS, 285, 640
Kurtz D. W. et al., 2011, MNRAS, 414, 2550
Ledoux P., 1951, ApJ, 114, 373
Loumos G. L., Deeming T. J., 1978, BAAS, 10, 417
O'Toole S. J., Jordan S., Friedrich S., Heber U., 2005, A&A, 437, 227
Pablo H., Kawaler S. D., Green E. M., 2011, ApJ, 740, L47
Paxton B., Bildsten L., Dotter A., Herwig F., Lesaffre P., Timmes F., 2011, ApJS, 192, 3
Pérez F., Oreiro R., Hu H., 2011, A&A, 535, A96
Pesnell W. D., 1985, ApJ, 292, 238
Reed M. D. et al., 2011, MNRAS, 412, 371
Reed M. D. et al., 2011, MNRAS, 414, 2885
Reed M. D., Foster H., Telting J. H., Østensen R. H., Farris L. H., Oreiro R., Baran A. S., 2014, MNRAS, 440, 3809

Telting J. H. et al., 2012, A&A, 544, A1
Telting J. H. et al., 2014, A&A, 570, A129
Zong W., Charpinet S., Vauclair G., 2016, A&A, 594, A46
Østensen R. H., Telting J. H., Reed M. D., Baran A. S., Nemeth P., Kiaeerad F., 2014, A&A, 569, A15

SUPPORTING INFORMATION

Supplementary data are available at *MNRAS* online.

Table 1. Excerpt of the full list of KIC 11558725's periodicities.

This paper has been typeset from a TEX/LATEX file prepared by the author.